Int J Biometeorol (2014) 58:2031–2043
DOI 10.1007/s00484-014-0804-x

ORIGINAL PAPER

Improvement in the accuracy of back trajectories using WRF to identify pollen sources in southern Iberian Peninsula

M. A. Hernández-Ceballos · C. A. Skjøth · H. García-Mozo · J. P. Bolívar · C. Galán

Received: 15 November 2013 / Revised: 10 February 2014 / Accepted: 11 February 2014 / Published online: 5 April 2014

Abstract Airborne pollen transport at micro-, meso-gamma and meso-beta scales must be studied by atmospheric models, having special relevance in complex terrain. In these cases, the accuracy of these models is mainly determined by the spatial resolution of the underlying meteorological dataset. This work examines how meteorological datasets determine the results obtained from atmospheric transport models used to describe pollen transport in the atmosphere. We investigate the effect of the spatial resolution when computing backward trajectories with the HYSPLIT model. We have used meteorological datasets from the WRF model with 27, 9 and 3 km resolutions and from the GDAS files with 1 ° resolution. This work allows characterizing atmospheric transport of *Olea* pollen in a region with complex flows. The results show that the complex terrain affects the trajectories and this effect varies with the different meteorological datasets. Overall, the change from GDAS to WRF-ARW inputs improves the analyses with the HYSPLIT model, thereby increasing the understanding the pollen episode. The results indicate that a spatial resolution of at least 9 km is needed to simulate atmospheric flows that are considerable affected by the relief of the landscape. The results suggest that the appropriate meteorological files should be considered when atmospheric models are used to characterize the atmospheric transport of pollen on micro-, meso-gamma and meso-beta scales. Furthermore, at these scales, the results are believed to be generally applicable for related areas such as the description of atmospheric transport of radionuclides or in the definition of nuclear-radioactivity emergency preparedness.

Keywords Back trajectories · Atmospheric models · HYSPLIT · WRF · *Olea* pollen · Southern Spain

Electronic supplementary material The online version of this article (doi:10.1007/s00484-014-0804-x) contains supplementary material, which is available to authorized users.

M. A. Hernández-Ceballos · J. P. Bolívar
Department of Applied Physics, University of Huelva, Huelva, Spain

C. A. Skjøth
National Pollen and Aerobiology Research Unit, Institute of Science and the Environment, University of Worcester, Worcester, UK

H. García-Mozo · C. Galán
Department of Botany, Ecology and Plant Physiology, Agrifood Campus of International Excellence (CeiA3), University of Córdoba, Córdoba, Spain

Present Address:
M. A. Hernández-Ceballos (✉)
European Commission, Joint Research Centre, Institute for Transuranium Elements, Nuclear Security Unit, Ispra, Italy
e-mail: miguelhceballos@gmail.com

Introduction

Pollen grains released to the air are dispersed and advected in the atmosphere due to spatial and temporal variations in meteorological conditions (Jones and Harrison 2004; Sousa et al. 2008). Due to their shape and size, this transport can be also affected by the physical characteristics of the pollen grains (Seinfield and Pandis 2006). Independent of some smaller pollen grains, they usually have a diameter in the range from ~20 μm (i.e. birch or ragweed pollen) to ~100 μm (i.e. maize or pine pollen). Settling velocities of pollen are substantial, generally varying from 1 to 30 cm/s (Aylor 2002). This means that both the physical properties of the atmosphere and the pollen grains determine the airborne pollen transport from the source (e.g. Jarosz et al. 2003; Arritt et al. 2007).

The key parameter of pollen transport is the atmospheric lifetime. The lifetime has a direct connection to the spatial and temporal scales of the distribution of pollen grains in the atmosphere and their variations with time (Seinfield and

Pandis 2006). In the case of pollen, it can be from less than an hour to several days, mainly due to substantial gravitational sedimentation. Most pollen grains from anemophilous plants are released passively under the influence of wind and turbulence (Michel et al. 2010). Recent studies suggest that depending on the height of the plant, thus affecting the release height of pollen grains (trees or weeds/grasses), the most relevant spatial scales for pollen dispersal are micro-, meso-gamma and meso-beta scales (Skjøth et al. 2013). The meso-alpha scale (200–2,000 km) covers long distance transport and must, however, not be neglected (e.g. Sofiev et al. 2006; Izquierdo et al. 2011; Zemmer et al. 2012).

Studies on airborne pollen must include atmospheric model tools to understand the underlying atmospheric processes (e.g. Prtenjak et al. 2012; Sofiev et al. 2013; Schueler and Schlünzen 2006; Zink et al. 2012). The application of these tools increases the understanding of pollen transport compared to the use of ground-based meteorological observations (e.g. García-Mozo et al. 2008). The computation of backward trajectories is widely used (Skjøth et al. 2009; Smith et al. 2008), where the Hybrid Single Particle Lagrangian Integrated Trajectory (HYSPLIT) model (Draxler et al. 2013) is one of the most used tools to explain atmospheric transport of pollen (e.g. Makra et al. 2010; Zemmer et al. 2012; Fernández-Rodriguez et al. 2014; Sikoparija et al. 2013).

The accuracy of atmospheric transport models, like HYSPLIT, is largely determined by the spatial resolution in the meteorological datasets (e.g. Skjøth et al. 2002). The spatial resolution has a direct effect on the quality of the simulations and, therefore, also the interpretations of the analysed episodes (Skjøth et al. 2002). In the case of pollen, this has special relevance in areas with complex terrain in which the pollen transport is widely governed by complex flows (e.g. Prtenjak et al. 2012). Two examples of complex flows are see-breeze effects or mountain valley effects. The horizontal scale of these effects is typically within the meso-gamma scale (2–20 km) or meso-beta scale (20–200 km). To study a certain spatial scale with meteorological models, a rule of thumb is that the meteorological model must have five grid points within the desired scale, which suggest that the meso-beta scale processes can be described with models that has 4–40 km distance between the grid points, whilst meso-gamma requires much higher resolution. These scales are still rare in operational meteorological models that are used for air quality studies. Therefore, it is necessary to consider the spatial resolution of the meteorological input data that is used. These considerations must include the scale of the atmospheric transport distance for each particular study (Veriankaite et al. 2010).

The atmospheric transport model HYSPLIT allows for both online and offline calculations. Online calculations with HYSPLIT are usually done by using the Global Data Assimilation System (GDAS) meteorological dataset (http://ready.arl.noaa.gov/HYSPLIT.php). The GDAS covers a decade, from 2004 to 2013. This is a big advantage in many aerobiological studies as they often spans 5 years or more (e.g. Orlandi et al. 2010; Skjøth et al. 2012). Another advantage is that 10 years of high-resolution meteorological data requires many computational resources to produce and store. A disadvantage is that the spatial resolution of the GDAS is more than 100 km. This means that the GDAS does not include specific atmospheric processes in relation to the meso-gamma scale and almost no processes on the meso-beta scale. It is therefore important to quantify the effect of using coarse scale meteorological datasets, like the GDAS, compared to higher resolution datasets, when atmospheric models, like HYSPLIT, are used in aerobiological studies. This has so far not been done in relation to aerobiology.

This paper examines the sensitivity of different input meteorological datasets in relation to trajectory models by using the most popular model in aerobiology, the HYSPLIT model, to characterize pollen transport in the atmosphere on the mesoscale. To meet this aim, this work compares trajectories obtained with HYSPLIT by using three high-resolution outputs from the mesoscale Weather Research and Forecasting (WRF-ARW) model (Skamarock et al. 2005) and GDAS datasets.

An *Olea* (olive tree) pollen episode recorded in Cordoba City, southern Iberian Peninsula (IP), has been selected as the case study. The episode was recorded outside of the local flowering period. This ensures that the episode is mainly due to atmospheric transport from remote sources. The episode has been analysed with the HYSPLIT model by using four different meteorological datasets, each with different spatial resolutions. Furthermore, the episode is analysed by using 3D simulations with the WRF model to explain the overall atmospheric conditions during the episode. The selection of this pollen species is based on two facts: (1) *Olea* pollen is the major cause of allergy in southern Spain (D'Amato et al. 1998; De Linares et al. 2007) and (2) *Olea* is the most important species from the agronomic and economic point of view in the Mediterranean area (IOC 2011). The present study determines the meteorological conditions and topographic main sources of *Olea* pollen that cause an increase in airborne pollen concentration out of the main pollen season. These results will be taken into account for producing pollen forecasts as well as related areas such as the description of atmospheric transport of radionuclides when the focus is the meso-gamma and meso-beta scales up to 200 km from the source.

Materials and methods

Study area and pollen concentrations

Daily and bi-hourly pollen data for the year 2010 were recorded in the city of Córdoba (37 ° 50′ N, 4 ° 45′ W, 120 m

above sea level (m.a.s.l.). Cordoba belongs to the Andalusia region in Spain and is located on the cultivated plain of the Guadalquivir (Fig. 1a). The Guadalquivir Valley, by a uniform height along it of less than 100 m.a.s.l., is bordered to the North by the Sierra Morena (mean height between 200 and 600 m.a.s.l.) and to the south and east by the Subbetic system (with heights around 2,000 m.a.s.l.), which are dominated by olive orchards (Fig. 1b). The entire distribution of olive crop in Andalucia provides a south–north and east–west gradient of *Olea* pollen sources around the Cordoba Province, with minimal presence in the north and west and a large source area located in the south and east.

Additionally, pollen data from "El Cabril" (38 ° 4′ N, 5 ° 24′ W, 450 m.a.s.l.), located 60 km north-west far away of Cordoba City (Fig. 1b), was included in order to determine if medium distance regions can contribute as source regions given that it registers high concentrations out of the Cordoba *Olea* main pollen season. In addition, pollen observations at Huelva (37 ° 16′ N, 6 ° 75′ W, 15 m.a.s.l.) and Seville (37 ° 25′ N, 5 ° 54′ W, 18 m.a.s.l.) were used to understand the pollen transport along the Guadalquivir Valley. A volumetric Hirst-type spore-trap (Hirst 1952) was used for pollen monitoring, and the daily and bi-hourly pollen count was produced using a microscope and visual detection for *Olea* pollen. The pollen concentrations were then calculated using the standardized data management procedures, following the rules laid down by the Spanish Aerobiology Network (REA) (Galán et al. 2007). During the studied period, field phenological observations were taken by using the phenological key developed by Maillard (1975). These field data offer information about the main *Olea* flowering season in Cordoba City surroundings.

Observations of wind direction and wind speeds were obtained from the Cordoba meteorological station, belonging to the Andalusia Government Agroclimatic Information Network (RIA). These parameters were used in combination with model calculations to characterize wind behaviour during the analysed episodes with high pollen concentrations.

Model overview and evaluation procedure

The HYSPLIT model was used to compute hourly 3D trajectories in a similar way as Hernández-Ceballos et al. (2011) and Harris et al. (2005). This methodology includes calculation of hourly 3D backward trajectories at five different heights: 100, 300, 500, 700 and 1,000 above ground level (agl), respectively.

The input to the HYSPLIT model was obtained from either the GDAS datasets or calculations with the WRF-ARW model. The GDAS files were obtained from the HYSPLIT online system and have 1 ° of spatial resolution, 24 levels of vertical resolution and 3 h of temporal coverage. The meteorological data are linearly interpolated from the analysis times to the trajectory computation time. The WRF-ARW files were available in three different spatial resolutions and a temporal resolution of 1 h. The files were created by using the following setup of the WRF model over the study region. Initial and boundary conditions to WRF were from FNL global analysis, created and maintained by the National Centres for Environmental Prediction (NCEP). The FNL data has a spatial resolution of 1 ° in latitude and longitude and a vertical resolution of 27 pressure levels.

To obtain the WRF files, three domains were defined using a two-way nesting strategy and a vertical structure that includes 40 sigma levels (Fig. 2). Two-way nesting has been used in several studies in IP, as Borge et al. (2008) or Carvalho et al. (2012). The model domain (D1) had a 27-km spatial resolution, and it covered western Europe, from the south of France to the north of Africa and a longitude from the western Mediterranean to the Canary Islands. The two nested domains had a spatial resolution of 9 km (D2) and 3 km (D3), respectively, where D3 covered the southwest of the IP. The WRF model used 24 h as spin-up time to allow the meteorological fields in the model to adjust the large-scale flow to the local topography, land use and other variables. Table 1 shows the

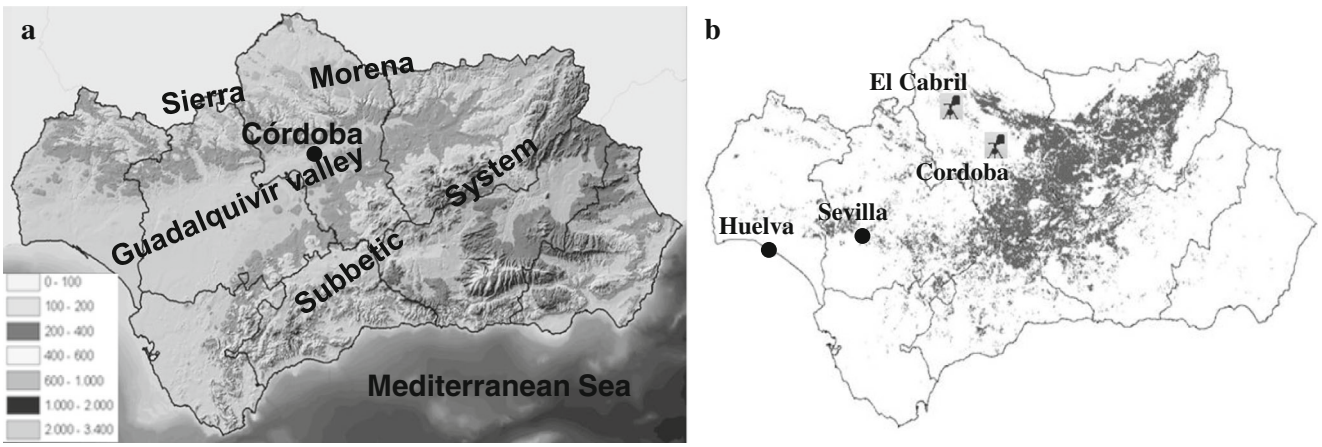

Fig. 1 **a** Area topography and **b** location of the study site, the *grey area* representing the olive crop distribution in Andalucia

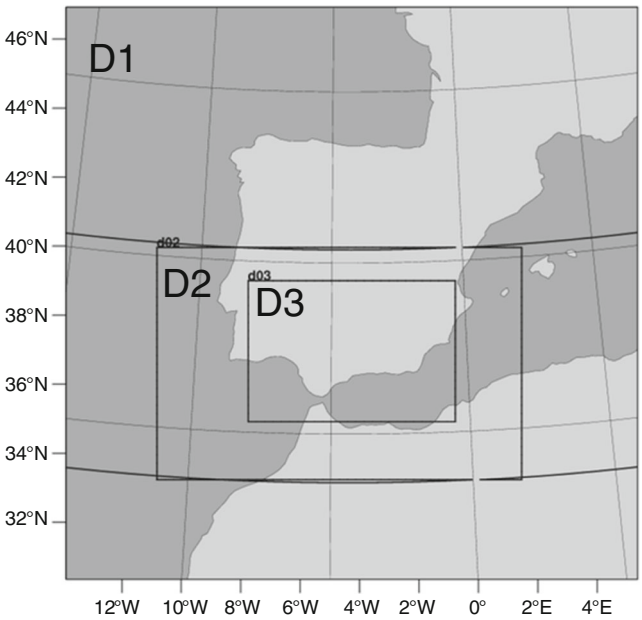

Fig. 2 WRF modelling domains (Lambert Conformal projection): domain D1 is coarse with resolution of 27 km, the D2 has a resolution of 9 km, whilst the finer D3 has a resolution of 3 km

information on the chosen physical options (identical for the three domains) in the WRF model for this study.

In the "Results" section, model results with GDAS or WRF are named individually, so that WRF-27 represents the results obtained from D1 (27 km), WRF-9 from D2 (9 km) and WRF-3 from D3 (3 km). The root mean square error (RMSE) and the bias score (BIAS) were used in the evaluation of the model results (Table 2), following the methodology shown in Jiménez-Guerrero et al. (2008) by using hourly data. Additionally, several statistical parameters were used to measure the sensitivity of trajectories. These parameters are the absolute horizontal transport deviation (AHTD), the absolute vertical transport deviation (AVTD) and the relative horizontal transport deviation (RHTD). All of them have been applied in earlier studies (Stohl and Seibert 1998; Harris et al. 2005).

Table 1 Details of the grids and the physics options fixed (identical in the three domains) in the WRF-ARW

	Domains		
	Domain 1	Domain 2	Domain 3
Horizontal resolution (km)	27	9	3
Vertical resolution	40 sigma levels		
Topography information	US Geological Survey (USGS) global 30 arc-second elevation (GTOPO30) dataset (Gesch and Larson 1996)		
Radiation	Dudhia (1989) scheme for shortwave radiation, rapid radiative transfer model (RRTM) for longwave radiation		
Surface processes	5-layer soil diffusion scheme (Dudhia 1996)		
Boundary layer	Yonsei University (YSU) (Hong et al. 2006)		
Cumulus	A modified version of the Kain and Fritsch (1990, 1993)		

Description of the investigated period

We studied the *Olea* airborne pollen "episode day" from 6 to 7 June 2010. In this period, pollen concentrations peaked outside the typical hours for flowering (11:00–17:00 UTC) (Galán et al. 1991). In addition, our episode was recorded outside the local *Olea* flowering period in the Córdoba Province. According to the phenological survey, in 2010, the flowering period in Cordoba City spread from April 24th until May 10th. In the southern part of the province, the flowering in Baena took place from the 14th to 28th of May and in Priego de Cordoba from May 21st to June 4th. Phenological records therefore insure that airborne pollen in Cordoba is external during this period of time, offering the possibility to trace associated pollen transport routes with atmospheric transport models.

Olea pollen concentrations reached a daily average of 314 pollen grains/m^3 on 6th and 376 pollen grains/m^3 on the 7th. The bi-hourly values showed that concentrations on the 6th were relatively constant, with values around 200–300 pollen grains/m^3, whilst on the 7th of June, there were two intensive peaks at 01:00–02:00 UTC and at 07:00–08:00 UTC (Fig. 3a) reaching 1,000 and 1,100 pollen grains/m^3, respectively. Pollen count declined sharply later with concentrations below 100 pollen grains/m^3.

The synoptic conditions over the IP included an anticyclone located to the west of IP and a low pressure system over the British Isles. This meteorological scenario can coincide with the development of a thermal low over the Iberian Peninsula plateau (Hoinka and De Castro 2003) (Fig. 3b), characterized by strong pressure gradients that occur at the periphery of the low causing low-level winds to blow from the coastal zones towards the interior of the peninsula. However, the influence of these thermal lows on the establishment and evolution of mesoscale processes is in general minimal in the area around the Guadalquivir Valley. Under this stable synoptic condition, the measured surface winds (Fig. 3a) over Cordoba City were mainly from the southwest with low intensity (less than 2 m/s). This constant arrival of southwesterly flows is due to the location of Cordoba City in the Guadalquivir Valley, which canalizes winds along its axis west/southwest–northeast, and hence, the surrounding topographic completely controls the wind direction at this site (Hernández-Ceballos et al. 2013).

Table 2 Bias score (BIAS) and root mean square error (RMSE) values for wind direction and speed at Cordoba site during 6–7 June 2010

	Wind direction (°)				Wind speed (m/s)			
	WRF (27 km)	WRF (9 km)	WRF (3 km)	GDAS (111 km)	WRF (27 km)	WRF (9 km)	WRF (3 km)	GDAS (111 km)
BIAS	4.31	7.92	−6.72	57.61	1.21	1.41	1.41	2.02
RMSE	62.24	87.56	66.29	77.49	2.23	2.22	2.23	2.35

Results

Comparison of simulated variables

The simulated values of wind direction showed larger variability than the observed values (Fig. 4). WRF simulations reproduced the arrival of southwestern winds during the daytime fairly well, whilst at night, from 00:00 to 06:00 UTC, they did not predict the wind observations that remained in a westerly range. Instead, WRF simulated the arrival of northeasterly flows. This behaviour was also observed in the GDAS values. The statistical values of BIAS indicated an underestimation of wind direction (−6.72 °) of WRF-3 and overestimation in the other cases, with the largest value obtained for GDAS values (57, 61 °). In the case of the RMSE, the results ranged between 60 ° and 90 °, registering the lowest value for WRF-27 (62 °) and the largest for WRF-9 with 87 °.

In general, WRF simulations did not reproduce the intensity and variability of wind speeds during the episode. The largest differences were observed during the afternoon of the last day with values up to 5 m/s. In general, both WRF and GDAS simulations overestimated the wind speeds with up to 2.0 (BIAS in GDAS) and 1.2–1.4 m/s (BIAS in WRF). The RMSEs were similar for both GDAS and WRF simulations,

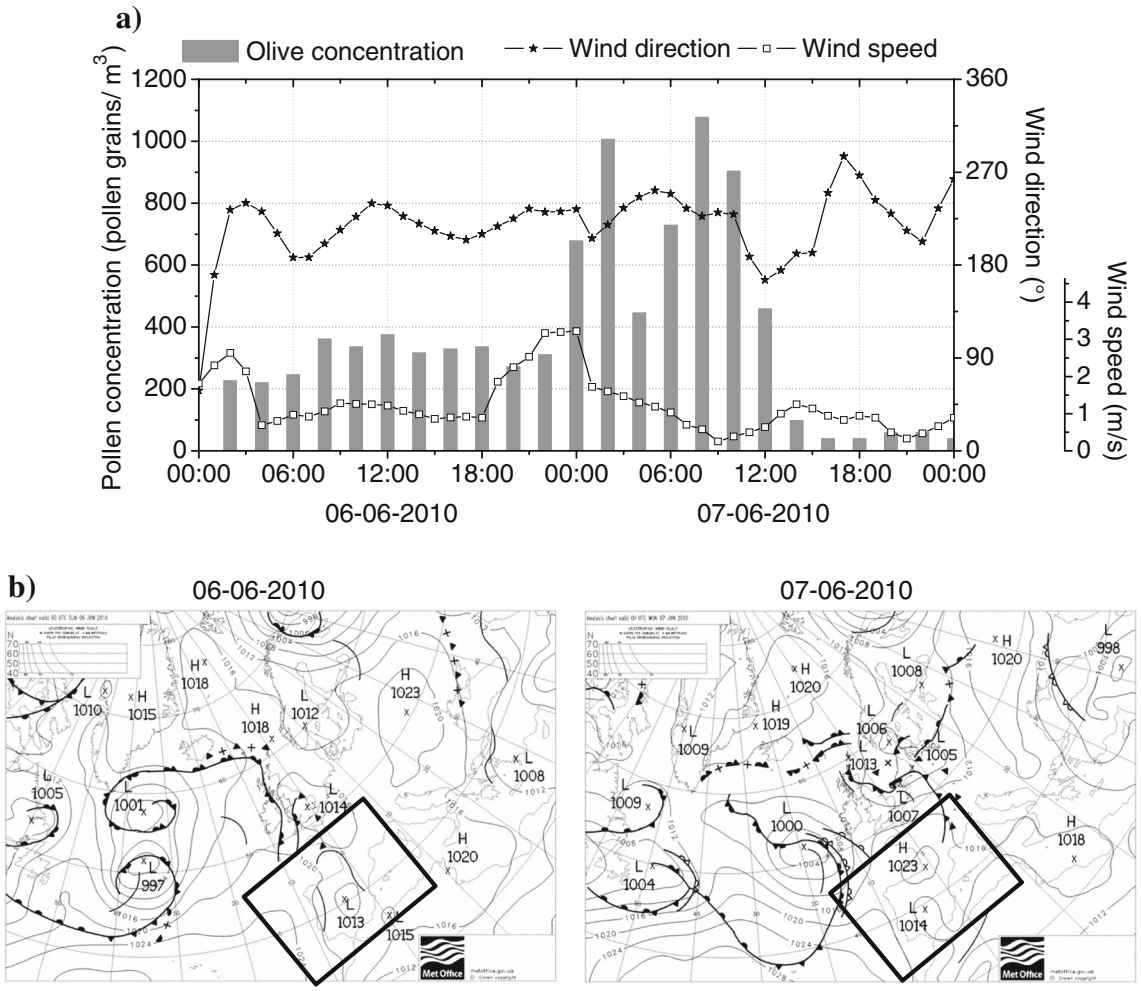

Fig. 3 **a** Hourly evolution of pollen concentrations, wind direction and speed at Córdoba City and **b** synoptic charts on 6–7 June 2010

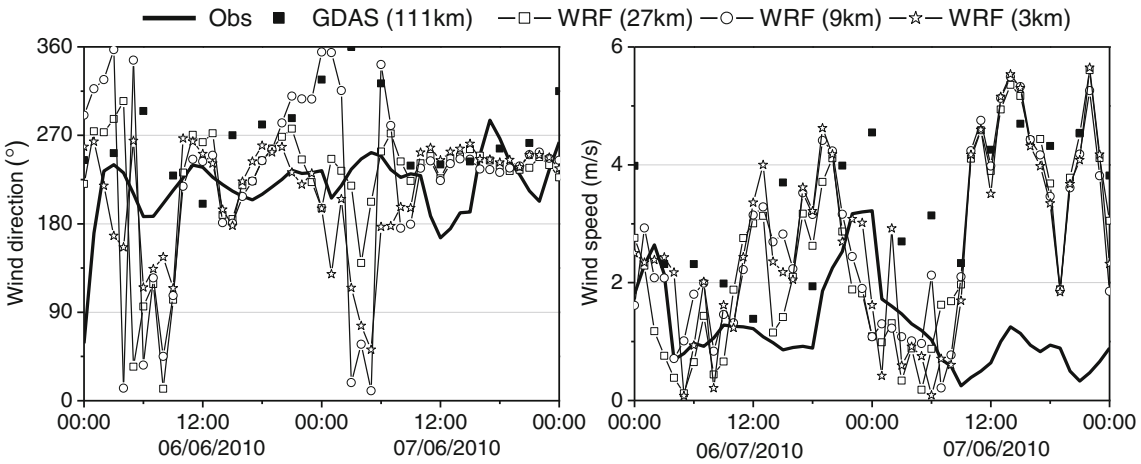

Fig. 4 Simulated and observed wind direction and speed at Cordoba City on 6–7 June 2010

reaching the maximum value for GDAS with 2.3 m/s and the minimum for WRF-9 with 2.2 m/s.

Backward trajectory analysis: variation with altitude

Figure 5 displays five different rows of 28-h back trajectories at five altitudes 100, 300, 500, 700 and 1,000 m.a.g.l., respectively. From left to right, the columns show increasing resolution in the meteorological data, from the GDAS datasets and WRF-27, WRF-9 and WRF-3 meteorological files, respectively. Each figure contains 24 back trajectories: one for each hour thus covering the period from 6th June 2010 (18:00 UTC) to 7th June 2010 (18:00 UTC).

The results showed that WRF results presented larger variability between different heights than GDAS. A good example is seen by comparing column 1 with column 4. In the case of GDAS, the trajectories showed a similar behaviour in all the heights, with a progressive displacement of the origin of air masses from the northwest to the north of Cordoba City, followed by a north–south movement until reaching the Guadalquivir Valley, which canalized in a southwest direction the flows to Cordoba City.

In contrast to this similar behaviour, the WRF back trajectories presented a clear variation in the results between each height. This observed variation on the trajectories with increasing height also changed with the spatial resolution. As an example, at 100 m, the WRF-27 and WRF-9 results displayed two clear behaviours of air masses during the period. The air masses flow along the Guadalquivir Valley from the afternoon of the 6th of June and until night (00:00 UTC). This valley flow was replaced by northern flows over Cordoba City from night until 9:00 UTC. After 09:00 UTC, the trajectories showed air mass movements along the Guadalquivir Valley again. This temporal variability was less prominent using the WRF-3 simulations. In the WRF-3 simulations, there was a much more constant air mass flow along the Guadalquivir Valley and only a few hours with the observed northern flow.

At 300 m, the results were similar to 100 m for WRF-27 and WRF-9. However, WRF-3 presented an increase in the number of trajectories that show air mass movements from the north. This tendency was also observed at 500 m. The results at 300 and 500 m showed a tendency to increase the spatial variability in the air mass pathways with increasing height. This suggests a reduction of wind canalization along the Guadalquivir Valley when increasing height. A consequence is that at these heights, a change in the origin of air masses using WRF-9 (at 500 m) and WRF-3 (at 300 and 500 m) was obtained, where the origin is the southern Atlantic coast of IP. This local valley flow is not present in either GDAS or WRF-27.

The increase in the variability of air masses with the height was confirmed at 700 m. The results of WRF-27 presented a wider range of air mass origins, whilst the WRF-9 and WRF-3 presented the influence of flows with southern movement. This larger variability increased the limitation in the identification of wind canalization along the valley. Finally, at 1,000 m, there are no arrivals of northern flows. At 1,000 m, the advection of flows is dominated by west-south movements. In this sense, the arrival of southerly flows was more observed in the results of WRF-9 and WRF-3. The channelization of air mass flows was therefore difficult to detect at 1,000 m.

Summarizing, the WRF meteorological files displayed a progressive increase in the spatial variability of air mass pathways and origins with increasing height. It has not been observed in the GDAS data. The trajectory results with WRF showed three air mass movements during the sampling period: (1) along the Guadalquivir Valley until midnight, (2) from the north until early morning and (3) and again along the valley from early morning and until the end of the day. These changes could not be obtained with the GDAS data. The causes to these changes are explained by the atmospheric dynamics and overall

Fig. 5 Hourly 28-h backward trajectory results at Cordoba City from 6 ▶ June 2010 at 18:00 UTC to 7 June 2010 at 18:00 using WRF outputs and GDAS files at **a** 100 m, **b** 300 m, **c** 500 m, **d** 700 m and **e** 1,000 m

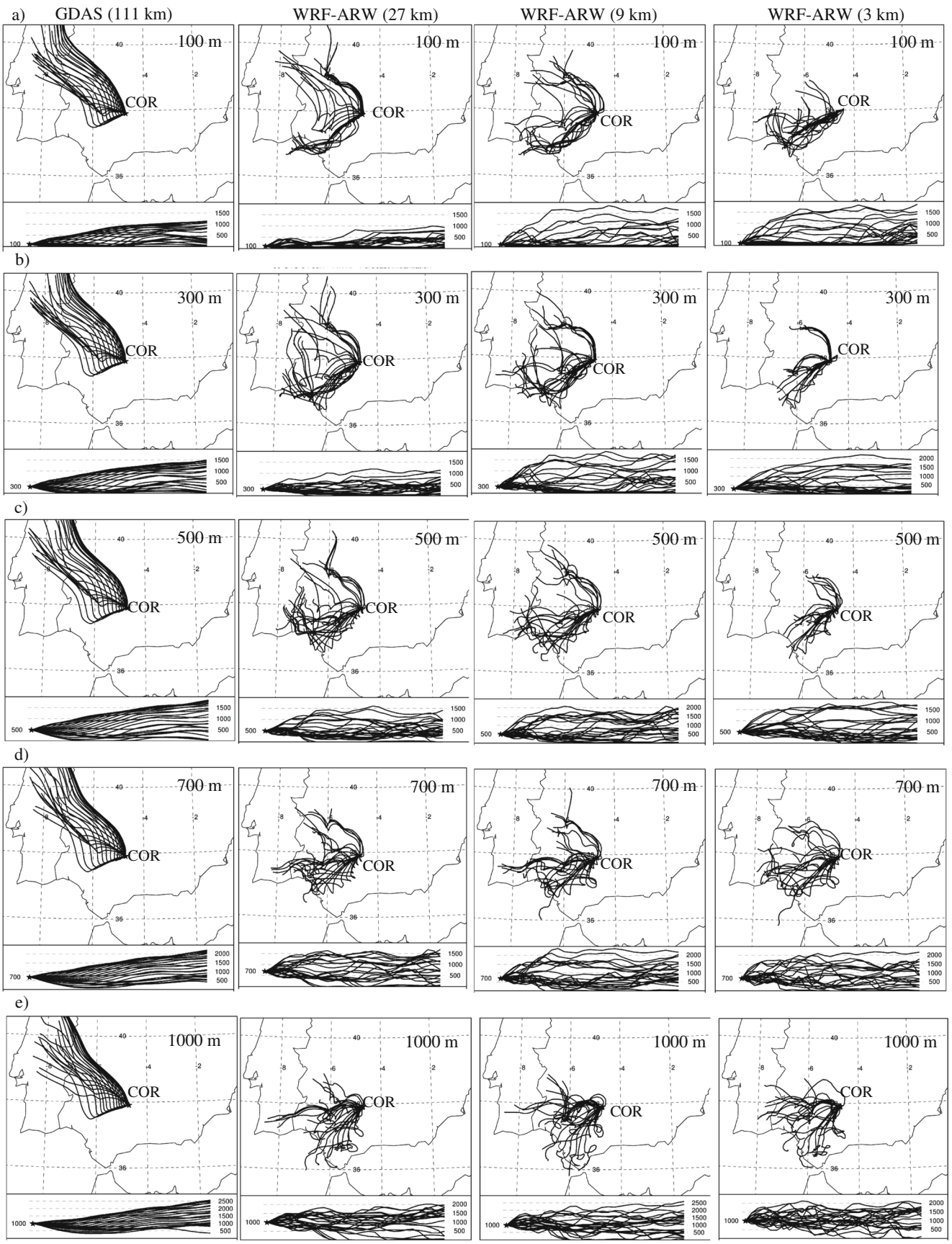
a)
GDAS (111 km)
WRF-ARW (27 km)
WRF-ARW (9 km)
WRF-ARW (3 km)
100 m
300 m
500 m
700 m
1000 m
COR
b)
c)
d)
e)

meteorological situation in the Guadalquivir Valley, shown in detail in the Supplementary information (Figs. S4 and S5) by using the results from WRF-3. This fact includes a cross section of the horizontal (u) wind component (isotachs) and specific humidity along the Guadalquivir Valley and along the northwest–southeast province axis.

The RHTD results (Table 3) showed a general increase in the uncertainty when the differences between the spatial resolutions were high. The uncertainty between GDAS and WRF trajectories was always higher than 40 %. This difference increased from GDAS–WRF-27 to GDAS–WRF-3, ranged between 51 and 64 % and reached the maximum value at 300 m. On the other hand, the uncertainty between WRF trajectories did not exceed 34 %. The smallest difference was between WRF-27 and WRF-9 (9–12 %) and the largest between WRF-9 and WRF-3 (9–30 %).

Regarding the AHTD index, the differences were always greater than 110 km between GDAS and WRF trajectories. The largest difference was obtained at 1,000 m, with around 150 km. In the case of WRF trajectories, there was a high similarity between WRF-27 and WRF-9. The difference ranged between 23 and 32 km. The maximum uncertainty was obtained again comparing WRF-9–WRF-3 with 16 km at 500 m and 70 km at 100 m. This behaviour among the trajectories was also observed in the AVTD index. The maximum values were registered between GDAS and WRF results. These differences ranged between 299 and 787 m and reached the maximum differences at 700 m. However, the vertical uncertainty for WRF trajectories showed a mean value smaller than 400 m. The largest differences were observed at low heights for the trajectories: at 500 m for WRF-27–WRF-9, at 300 m for WRF-27–WRF-3 and at 100 m for WRF-9–WRF-3.

Figure 6 displays the graphical evolution of AHTD and AVTD statistics in time along the trajectory until 28 h back at 100, 500 and 1,000 m. The results obtained at 300 and 700 m displayed similar behaviour and are therefore not shown.

The results showed that deviations between GDAS and WRF data were larger than the difference between WRF trajectories that were obtained with different spatial resolutions. The RHTDs, caused by the differences between GDAS and WRF trajectories (black and dashed lines), started with small values and accumulated with a lineal increase over time at each height. The largest slopes were seen in the case of 1,000 m and reached at this height similar values around 300 km at the end of the period. On the other hand, the RHTDs associated with the differences between WRF trajectories (lines with symbols) showed a small increase over time, not exceeding at last time the value of 150 km. This figure clearly showed that the deviations obtained among the GDAS–WRF results were much larger than those for between the different WRF datasets.

Figure 6 also shows that vertical deviations (AVTDs) associated to different horizontal spatial resolutions started with small values and increased over time. This fact displays the presence of elevated areas causing the air masses to rise quickly. Deviations when comparing GDAS with WRF trajectories were again usually larger than deviations between the different WRF options. In general, the WRF results presented a similar behaviour with height with a general tendency to increase the value of the AVTD index over time although with periods where the vertical deviation registered very similar values. In this case, the maximum value reached was around 600 m at the end of the period.

Table 3 Comparison of 28-h back trajectories at Cordoba by calculating transport difference in trajectories by using different meteorological datasets

		100 m	300 m	500 m	700 m	1,000 m
GDAS and WRF-27	RHTD (%)	45	42	41	46	55
	AHTD (km)	116	120	117	127	151
	AVTD (m)	299	487	599	716	626
GDAS and WRF-9	RHTD (%)	50	44	46	48	56
	AHTD (km)	129	121	124	132	158
	AVTD (m)	323	605	687	761	657
GDAS and WRF-3	RHTD (%)	52	64	55	51	57
	AHTD (km)	138	133	129	140	154
	AVTD (m)	479	639	693	787	584
WRF-27 and WRF-9	RHTD (%)	9	12	12	11	12
	AHTD (km)	22	32	28	23	28
	AVTD (m)	93	253	261	176	228
WRF-27 and WRF-3	RHTD (%)	34	29	17	19	17
	AHTD (km)	79	57	33	40	32
	AVTD (m)	374	399	278	341	290
WRF-9 and WRF-3	RHTD (%)	30	20	9	19	12
	AHTD (km)	70	37	16	40	24
	AVTD (m)	386	308	168	306	329

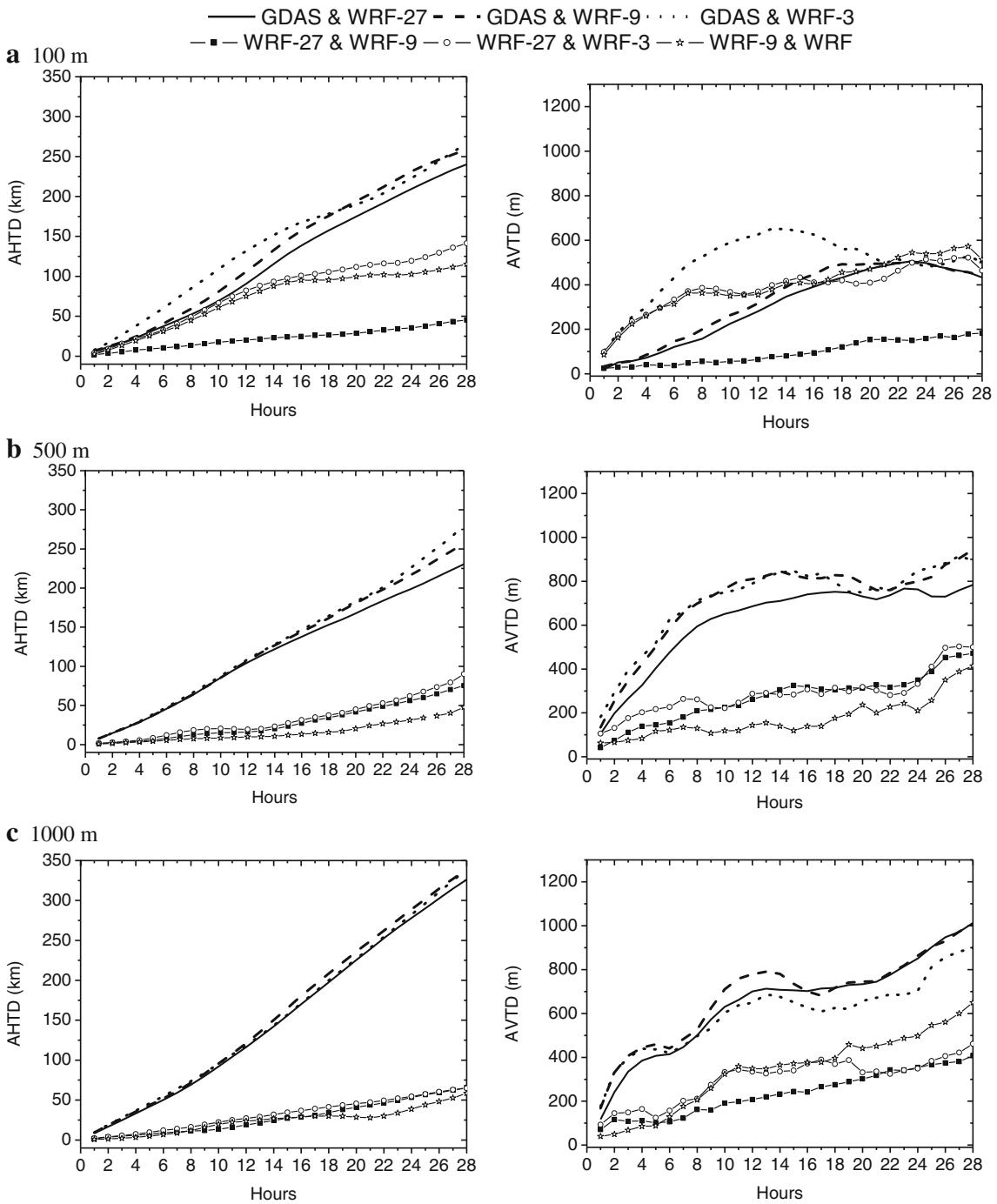

Fig. 6 Trajectory differences associated by dataset (GDAS and WRF meteorological files) at 100, 500 and 1,000 m corresponding to **a** AHTD, **b** RHTD and **c** AVTD, respectively

Discussion

The current study supports the hypothesis that the computation of backward trajectories as well as the characterization of meteorological conditions can vary depending on the use of different input meteorological datasets. Our results show that all statistical measures are better on the WRF data than on the GDAS data. The best statistical results are obtained using WRF-27, although there is a little difference between WRF-27, WRF-9 and WRF-3. In this sense, and focusing on the inner domain, the results for WRF-3 and WRF-9 are better than WRF-27 as WRF-9 and WRF-3 have a much better description of the valley flow and its changes throughout the day, although the actual wind speed is not that well described. This result is in agreement with previous results obtained that focus on the performance of the WRF model (Borge et al.

2008; Challa et al. 2009; Papanastasiou et al. 2010). These results indicate the ability of the WRF model to simulate wind direction in this site, located in a small valley inside the Guadalquivir Valley and close to the Sierra Morena mountains, but it can be an overestimation of local wind speeds when the model is compared to observations from the city. The largest bias is observed when wind speeds are generally less than 1 m/s. The difficulty in the simulation of wind speed has been observed in the case of the WRF model, increasing the bias of wind speed over plains and valleys (Jiménez and Dudhia 2012). This is a common problem of atmospheric boundary layer (ABL) schemes that use similarity theory, which is known to break down at very low wind speeds (e.g. Ha et al. 2007).

The results of backward trajectories display the influence by using meteorological data with different horizontal spatial resolutions. The AHTD and AVTD statistics have similar magnitudes to those found by Stohl and Seibert (1998) in their comparison of 3D vs. isentropic trajectories in the troposphere and in Harris et al. (2005). Both studies quantify the sensitivity of the trajectory model regarding the input meteorological data.

Large differences were observed between GDAS and WRF trajectories. In the case of GDAS, the trajectories show very similar behaviour with height. On the contrary, the WRF trajectories present a variation with height at all different spatial resolutions. The main reason behind these results is most likely the horizontal resolution of the meteorological data and how the topography affects especially the lower parts of the atmosphere (Fig. S1). Another important reason is related to the different parameterisations that are used in the two model formulations. Firstly, large differences in the relief of the landscape are seen from the digital elevation model over the southern Iberian Peninsula at each of the four different spatial resolutions. This representation plays a key role in the characterization of surface winds in this area. As an example, the valleys around the Cordoba region are only present in the 9- and 3-km resolutions. This affects directly how the physical processes are simulated with the WRF model. This is also illustrated by the AVTD statistical results with much higher variability for 3 and 9 km resolutions with distance than 27 and 111 km resolutions. The reason is that the vertical winds at 3 and 9 km are much more influenced by topography and complex flow than coarser resolution model calculations. Secondly, the large difference in grid resolution between WRF and GDAS results in a large difference in the use of physical parameterisations. In general, the purpose of parameterisation in an atmospheric model is to provide a statistical and mechanistic good description of physical processes that cannot directly be resolved directly with the chosen grid resolution. This means that the overall effect of valley processes that are directly simulated in the current model simulations with WRF will be incorporated by the use of parameterisation in the GFS model that provides the GDAS dataset. Due to the large difference in the processes that can be simulated with the two different grid resolutions (WRF and GFS), then there will be a considerable difference in the formulation of most parameterisations in the two models, especially in relation to precipitation and processes in the ABL. The choice (as well as behaviour) of such parameterisations is mainly determined by the grid resolution of the model (e.g. Wang and Coauthors 2014).

The differences in the trajectory results are important in the analysis of airborne material (including airborne pollen) at the meso-beta scale and also in the identification of source areas. During the sampling period, whilst WRF trajectories display two clear air mass displacements, the GDAS results are less clear. Therefore, for this particular episode, the connection between atmospheric transport and remote source regions is difficult to establish with GDAS data and much more straightforward by using WRF data, especially at 9 and 3 km spatial resolutions.

In this case, considering the origins and pathways of back trajectories, both the GDAS and WRF results would suggest source areas in a range from the north to the southwest of Cordoba City. Combining this knowledge with the geographical distribution of the sources and phenological characteristics of potential pollen source regions, the responsible sources from Cordoba can be defined. This study has a high temporal resolution pollen concentration data and it is possible to identify the origin of measured pollen at monitoring sites as described by Gassmann and Pérez (2006) and Makra et al. (2010).

These results suggest that the first pollen peak in Córdoba is related to northern flows associated to northern *Olea* pollen sources. Figure 1 shows only a small number of potential *Olea* sources in that part of the Cordoba Province. Field phenological observations indicate that *Olea* in the north of the province are during the flowering period. So it would be possible that these crops, together with favourable winds, are responsible of the first pollen peak at Cordoba City. To confirm this pollen transport, the hourly pollen evolution at El Cabril site is shown in Fig. S2, with a progressive increase in pollen concentrations from 15:00 UTC time and a maximum at 18:00 UTC time (80 pollen grains/m^3). This information ensures that the peak at El Cabril was reported 5 h later at Cordoba City.

The second peak, according to the trajectory analysis, is also connected with the progressive and constant arrival of air mass flows along the Guadalquivir Valley. These air masses pass the *Olea* sources located inside and in the north area of the valley. Therefore, the air masses and the airborne pollen are affected by the canalization of the air masses by the valley. Daily mean values from sampling sites along the valley (Seville and Huelva) reveal the presence of relative peaks on the 5th and 6th of June (Fig. S3). This fact supports the argument of atmospheric pollen transport along the valley

during the sampling period. Therefore, the second pollen peak at Cordoba City can be associated with the sum of (1) pollen transport along the valley and (2) arrival of northern air masses.

These results enlarge the typical footprint area of *Olea* crops with respect to *Olea* pollen count at Cordoba City including areas located in the west, along the Guadalquivir Valley and its surroundings. This footprint area is in general associated with a pollen transport on the meso-beta scale (20–200 km), according to the definition by Orlanski (1975). Therefore, this paper presents valuable results to produce pollen forecasts for Cordoba City, as they complement those previously obtained in the area that indicated the influence of different cultivated crops in the south of the province based on field phenological observations (Fornaciari et al. 2000; García-Mozo et al. 2005). In this respect, a recent study has demonstrated that *Olea* pollen can vary substantially in allergen release, even though they are morphologically identical (Galán et al. 2013). These variations might be related to either different source areas or to transformation of allergens during the 6–12-h atmospheric transport that is the typical atmospheric lifetime on the meso-beta scale.

This study indicates that regional sources should be considered in the aim of understanding the temporal pollen evolution and also their influence consisting of a mixture of atmospheric transport processes. These results are in agreement with those obtained in Aarhus (Denmark) for grass pollen concentrations (Skjøth et al. 2013). Nevertheless, the atmospheric transport of pollen at these scales is poorly understood, and the understanding and modelling of pollen transport that combines these scales has been identified as one of the major challenges for the modelling community (Sofiev et al. 2013).

Conclusions

The current study showed the benefits of using meteorological files with higher spatial resolution in the computation of back trajectories. Replacing GDAS data with WRF data have allowed us to identify *Olea* pollen source areas responsible of high pollen episodes in Cordoba City. The results have shown that the use of the mesoscale meteorological model WRF-ARW improves the accuracy of backward trajectories because the WRF model can take into account complex flows that play a key role in the Guadalquivir Valley.

The use of high spatial resolution has allowed a detailed analysis of the *Olea* pollen transport detected at Cordoba City, including transport along the Guadalquivir Valley, i.e. the nearest sources can be about 50–80 km away. The improvement in the analysis was mainly seen by using the WRF model results with 9 and 3 km resolutions. Results indicate that the use of appropriate meteorological files with high spatial resolution is important in back trajectory pollen studies. But they also suggest that incorporation of the relevant atmospheric scales, and also physical processes described with WRF, affects the pollen transport along the Guadalquivir Valley mainly detected with spatial resolutions at the 9- and 3-km resolutions.

Acknowledgments The authors are grateful to the European Social Fund and the Spanish Science Ministry for joint financing. Dr. García-Mozo was supported by a "Ramón y Cajal" contract. The Andalusia Regional Government funded the project entitled "Analisis de la Dinamica del Polen Atmosferico en Andalucia" (RNM-5958). Dr. Skjøth was supported by the Danish Research Council through the project SUPREME. The authors also thank the Science and Innovation Ministry for funding the project entitled "Impacto del Cambio Climatico en la Fenologia de especies vegetales del Centro y Sur de la Peninsula Iberica" (FENOCLIM) CGL2011-24146. Support from the EU FP7-HIALINE project is gratefully acknowledged. The authors gratefully acknowledge the NOAA Air Resources Laboratory (ARL) for the provision of the HYSPLIT transport and dispersion model used in this publication, to the Andalusia Government Agroclimatic Information Network (RIA) for providing meteorological observations for Cordoba, and to the ENRESA company for facilitating the pollen and meteorological study at the "El Cabril" station.

References

Arritt RW, Clark CA, Goggi AS, Lopez Sanchez H, Westgate ME, Riese JM (2007) Lagrangian numerical simulations of canopy air flow effects on maize pollen dispersal. Field Crop Res 102:151–162

Aylor DE (2002) Settling speed of corn (Zea mays) pollen. J Aerosol Sci 33:1601–1607

Borge R, Alexandrov V, Del Vas JJ, Lumbreras J, Rodriguez E (2008) A comprehensive sensitivity analysis of the WRF model for air quality applications over the Iberian Peninsula. Atmos Environ 42:8560–8574

Carvalho D, Rocha A, Gómez-Gesteira M, Santos C (2012) A sensitivity study of the WRF model in wind simulation for an area of high wind energy. Environ Model Software 33:23–34

Challa VS, Indracanti J, Rabarison MK, Patrick C, Baham JM, Young J, Hughes R, Hardy MG, Swanier SJ, Yerramilli A (2009) A simulation study of mesoscale coastal circulations in Mississippi Gulf coast. Atmos Res 91:9–25

D'Amato G, Spieksma G, Liccardi G, Jäger S, Russo M, Kontou-Fili K, Nikkels H, Wüthrich B, Bonini S (1998) Pollen-related allergy in Europe. Allergy 53:567–578

De Linares C, Nieto-Lugilde D, Alba F, Díaz de la Guardia C, Galán C, Trigoz MM (2007) Detection of airborne allergen (Ole e 1) in relation to Olea europaea pollen in S Spain. Clin Exp Allergy 37:125–132

Draxler RR, Stunder B, Rolph G, Taylor A (2013) HYSPLIT_4 user's guide. NOAA Air Resources Laboratory. http://www.arl.noaa.gov/documents/reports/hysplit_user_guide.pdf

Dudhia J (1989) Numerical study of convection observed during the winter monsoon experiment using a mesoscale two-dimensional model. J Atmos Sci 46:3077–3107

Dudhia J (1996) A multilayer soil temperature model for MM5. Preprints, Sixth PSU/NCAR Mesoscale Model Users Workshop, Boulder, CO, PSU/NCAR

Fernández-Rodriguez S, Skjøth C, Tormo-Molina R, Brandao R, Caeiro E, Silva-Palacios I, Gonzalo-Garijo Á, Smith M (2014)

Identification of potential sources of airborne *Olea* pollen in the Southwest Iberian Peninsula. Int J Biometeorol. doi:10.1007/s00484-012-0629-4

Fornaciari M, Galán C, Mediavilla A, Domínguez E, Romano B (2000) Aeropalynological and phenological study in two different olive Mediterranean areas: Córdoba (Spain) and Perugia (Italia). Plant Biosyst 134:199–204

Galán C, Tormo R, Cuevas J, Infante F, Domınguez E (1991) Theoretical daily variation patterns of airborne pollen in the southwest of Spain. Grana 30:201–209

Galán C, Cariñanos P, Alcázar P, Domínguez E (2007) Management and quality manual. Spanish Aerobiology Network (REA). Servicio Publicaciones Universidad de Córdoba, Córdoba, ISBN 978-84-690-6353-8

Galán C, Antunes C, Brandao R, Torres C, Garcia-Mozo H, Caeiro E, Ferro R, Prank M, Sofiev M, Albertini R, Berger U, Cecchi L, Celenk S, Grewling L, Jackowiak B, Jaager S, Kennedy R, Rantio-Lehtimaki A, Reese G, Sauliene I, Smith M, Thibaudon M, Weber B, Weichenmeier I, Pusch G, Buters JTM, on behalf of the HIALINE Working Group (2013) Airborne olive pollen counts are not representative of exposure to the major olive allergen Ole e 1. Allergy 68:809–812

García-Mozo H, Galán C, Vazquez L (2005) The reliability of geostatistic interpolation in olive field phenology. Aerobiologia 22:97–108

García-Mozo H, Galán C, Belmonte J, Bermejo D, Díaz de la Guardia C, Elvira B et al (2008) Regional phenological models to forecast the start and peak of *Quercus* pollen season in Spain. Agr Forest Meteorol 148:372–380

Gassmann MI, Pérez CF (2006) Trajectories associated to regional and extra- regional pollen transport in the southeast of Buenos Aires province, Mar del Plata (Argentina). Int J Biometeorol 50:280–291

Gesch DB, Larson KS (1996) Techniques for development of global 1-kilometer digital elevation models. Proc. Pecora 13th Symp. human interactions with the environment—perspectives from space, 13th, Sioux Falls, South Dakota, August 20-22, Proceedings: Bethesda, Maryland, American Society of Photogrammetry and Remote Sensing

Ha K-J, Hyun Y-K, Oh H-M, Kim K-E, Mahrt L (2007) Evaluation of boundary layer similarity theory for stable conditions in CASES-99. Mon Weather Rev 135:3474–3483

Harris JM, Draxler RR, Oltmans SJ (2005) Trajectory model sensitivity to differences in input data and vertical transport method. J Geophys Res 110, D14109. doi:10.1029/2004JD005750

Hernández-Ceballos MA, García-Mozo H, Adame JA, Domínguez-Vilches E, De la Morena BA, Bolívar JP, Galán C (2011) Synoptic and meteorological characterization of olive pollen transport in Cordoba province (South-western Spain). Int J Biometeorol 55:17–34

Hernández-Ceballos MA, Adame JA, Bolívar JP, De la Morena BA (2013) A mesoscale simulation of coastal circulation in the Guadalquivir valley (southwestern Iberian Peninsula) using the WRF-ARW model. Atmos Res 124:1–20

Hirst J (1952) An automatic volumetric spore-trap. Ann Appl Biol 36: 257–265

Hoinka KP, De Castro M (2003) The Iberian Peninsula thermal low. Q J Roy Meteorol Soc 129:1491–1511

Hong S-Y, Noh Y, Dudhia J (2006) A new vertical diffusion package with an explicit treatment of entrainment processes. Mon Weather Rev 134:2318–2341

IOC (2011). International Olive Council. http://www.internationaloliveoil.org/

Izquierdo R, Belmonte J, Avila A, Alarcón M, Cuevas E, Alonso-Pérez S (2011) Source areas and long-range transport of pollen from continental land to Tenerife (Canary Islands). Int J Biometeorol 55:67–85

Jarosz N, Loubet B, Durand B, McCartney A, Foueillassar X, Huber L (2003) Field measurements of airborne concentration and deposition rate of maize pollen. Agr Forest Meteorol 19:37–51

Jiménez PA, Dudhia J (2012) Improving the representation of resolved and unresolved topographic effects on surface wind in the WRF model. J Appl Meteor Climatol 51:300–316

Jiménez-Guerrero P, Jorba O, Baldasano JM, Gassó S (2008) The use of a modelling system as a tool for air quality management: annual high-resolution simulations and evaluation. Sci Total Environ 390:323–340

Jones AL, Harrison RM (2004) The effects of meteorological factors on atmospheric bioaerosol concentrations—a review. Sci Total Environ 326:151–180

Kain JS, Fritsch JM (1990) A one-dimensional entraining/detraining plume model and its application in convective parameterization. J Atmos Sci 47:2784–2802

Kain JS, Fritsch JM (1993) Convective parameterisation for mesoscale models: the Kain-Fritsch scheme. The Representation of Cumulus Convection in Numerical Models. Meteorol Monogr 24:165–170

Maillard R (1975) L'olivier. INVUFLEC, Paris

Makra L, Santa T, Matyasovszky I, Damialis A, Karatzas K, Bergmann KC, Vokou D (2010) Airborne pollen in three European cities: detection of atmospheric circulation pathways by applying three-dimensional clustering of backward trajectories. J Geophys Res Atmos 115, D24220. doi:10.1029/2010JD014743

Michel D, Gehrig R, Rotach MW, Vogt R (2010) MicroPoem: experimental investigation of birch pollen emissions. In: 29th conference on agricultural and forest meteorology, 19th symposium on boundary layers and turbulence, ninth symposium on the Urban Environment, Keystone, 2 - 6 August. http://www.meteoschweiz.admin.ch/web/de/forschung/publikationen/alle_publikationen/micropoem__experimental.html

Orlandi F, Garcia-Mozo H, Galán C, Romano B, Diaz de la Guardia C, Ruiz L, Trigo MM, Dominguez-Vilches E, Fornaciari M (2010) Olive flowering trends in a large Mediterranean area (Italy and Spain). Int J Biometeorol 54:151–163

Orlanski I (1975) A rational subdivision of scales for atmospheric processes. B Am Meteorol Soc 56:527–530

Papanastasiou DK, Melas D, Lissaridis I (2010) Study of wind field under sea breeze conditions; an application of WRF model. Atmos Res 98: 102–117

Prtenjak MT, Srnec L, Peternel R, Madžarević V, Hrga I, Stjepanović B (2012) Atmospheric conditions during high ragweed pollen concentrations in Zagreb, Croatia. Int J Biometeorol 56:1145–1158

Schueler S, Schlünzen K (2006) Modeling of oak pollen dispersal on the landscape level with a mesoscale atmospheric model. Environ Model Assess 11:179–194

Seinfield JH, Pandis SN (2006) Atmospheric chemistry and physics: from air pollution to climate change. Wiley, New York

Sikoparija B, Skjøth CA, Alm Kübler K, Dahl A, Sommer J, Grewling Radisic P, Smith M (2013) A mechanism for long distance transport of *Ambrosia* pollen from the Pannonian Plain. Agr Forest Meteorol 180:112–117

Skamarock WC, Klemp JB, Dudhia J, Gill DO, Barker DM, Wang W, Powers JG (2005) A description of the advanced research WRF version 2. NCAR Tech Notes-468+STR.

Skjøth CA, Hertel O, Ellermann T (2002) Use of the ACDEP trajectory model in the Danish nation-wide background monitoring programme. Phys Chem Earth A B C 27(35):1469–1477

Skjøth CA, Smith M, Brandt J, Emberlin J (2009) Are the birch trees in Southern England a source of *Betula* pollen for North London? Int J Biometeorol 53:75–86

Skjøth CA, Sommer J, Frederiksen L, Gosewinkel Karlson U (2012) Crop harvest in Denmark and Central Europe contributes to the local load of airborne Alternaria spore concentrations in Copenhagen. Atmos Chem Phys 12:11107–11123

Skjøth CA, Ørby PV, Becker T, Geels C, Schlunssen V, Sigsgaard T, Bønløkke JH, Sommer J, Søgaard P, Hertel O (2013) Identifying urban sources as cause of elevated grass pollen

concentrations using GIS and remote sensing. Biogeosciences 10:541–554

Smith M, Skjøth CA, Myszkowska D, Uruska A, Malgozata P, Stach A et al (2008) Long-range transport of Ambrosia pollen to Poland. Agr Forest Meteorol 148:1402–1411

Sofiev M, Siljamo P, Ranta H, Rantio-Lehtimaki A (2006) Towards numerical forecasting of long-range air transport of birch pollen: theoretical considerations and a feasibility study. Int J Biometeorol 50:392–402

Sofiev M, Siljamo P, Ranta H, Linkosalo T, Jaeger S, Rasmussen A, Rantio-Lehtimaki A, Severova E, Kukkonen J (2013) A numerical model of birch pollen emission and dispersion in the atmosphere. Description of the emission module. Int J Biometeorol 57:45–58

Sousa SIV, Martins FG, Pereira MC, Alvim-Ferraz MCM, Ribeiro H, Oliveira M, Abreu I (2008) Influence of atmospheric ozone, PM10 and meteorological factors on the concentration of airborne pollen and fungal spores. Atmos Environ 42:7452–7464

Stohl A, Seibert P (1998) Accuracy of trajectories as determined from the conservation of meteorological tracers. Q J Roy Meteorol Soc 12: 1465–1484

Veriankaite L, Siljamo P, Sofiev M, Sauliene I, Kukkonen J (2010) Modelling analysis of source regions of long-range transported birch pollen that influences allergenic seasons in Lithuania. Aerobiologia 26:47–62

Wang W, Coauthors (2014) ARW version 3.5 modeling system user's guide. NCAR Tech. Note, 413 pp., Natl. Cent. for Atmos. Res., Boulder, CO. [available from http://www.mmm.ucar.edu/wrf/users/]

Zemmer F, Karaca F, Ozkaragoz F (2012) Ragweed pollen observed in Turkey: detection of sources using back trajectory models. Sci Total Environ 430:101–108

Zink K, Vogel H, Vogel B, Magyar D, Kottmeier C (2012) Modeling the dispersion of *Ambrosia artemisiifolia* L. pollen with the model system COSMO-ART. Int J Biometeorol 56:669–680